

Water-stable, hydroxamate anchors for functionalization of TiO₂ surfaces with ultrafast interfacial electron transfer

William R. McNamara, Rebecca L. Milot, Hee-eun Song, Robert C. Snoeberger III, Victor S. Batista,* Charles A. Schmuttenmaer,* Gary W. Brudvig* and Robert H. Crabtree*

Received 18th January 2010, Accepted 8th March 2010

First published as an Advance Article on the web 26th April 2010

DOI: 10.1039/c001065k

A novel class of derivatized hydroxamic acid linkages for robust sensitization of TiO₂ nanoparticles (NPs) under various aqueous conditions is described. The stability of linkages bound to metal oxides under various conditions is important in developing photocatalytic cells which incorporate transition metal complexes for solar energy conversion. In order to compare the standard carboxylate anchor to hydroxamates, two organic dyes differing only in anchoring groups were synthesized and attached to TiO₂ NPs. At acidic, basic, and close to neutral pH, hydroxamic acid linkages resist detachment compared to the labile carboxylic acids. THz spectroscopy was used to compare ultrafast interfacial electron transfer (IET) into the conduction band of TiO₂ for both linkages and found similar IET characteristics. Observable electron injection and stronger binding suggest that hydroxamates are a suitable class of anchors for designing water stable molecules for functionalizing TiO₂.

1. Introduction

For dye-sensitized solar cells (DSSCs)^{1,2} and photocatalysis,^{3,4} wide band-gap semiconductors are commonly functionalized by covalently attaching molecules to the surface, allowing for visible light sensitization. These adsorbates (dyes) range from immobilized metal complexes to organic molecules that absorb a broad range of visible light. Photoinduced interfacial electron transfer (IET), the process responsible for advancing the oxidation state of these adsorbates, can then participate in the redox chemistry relevant to DSSCs or photocatalysis.^{5,6} Furthermore, the redox species in solution stabilizes the adsorbate by rapidly reducing the photooxidized surface complex, preventing recombination by making back electron transfer several orders of magnitude slower than the forward transfer. For stability and longevity of these systems, ensuring robustness and efficient electron injection under various aqueous conditions is important for designing the most efficient devices for solar energy applications. In this study, we describe the characteristics of hydroxamate anchors for functionalization of TiO₂ nanoparticles (NPs). A direct comparison is made between two molecules which differ only in the anchoring group showing that hydroxamic acids provide a more robust scaffold than carboxylic acids for designing molecules for sensitizing TiO₂.

The use of dyes exhibiting visible light absorption when attached to metal oxide surfaces has been pursued for electrocatalysis,⁷ photocatalysis,^{8,9} and solar energy storage.¹⁰ The molecular anchors which bind adsorbates to metal oxides in these systems are limited to a small number of functional groups which include alcohols,¹¹ carboxylic acids,^{2,8} silanes,¹² phosphonates,⁷ and acetylacetonate derivatives.¹³ The most successful and widely utilized dyes for DSSCs belong to a small group of ruthenium bipyridyl complexes that bind to TiO₂ through carboxylic acid functional groups.^{1,2} The carboxylic acid group forms bonds with TiO₂ that are stable in anhydrous conditions but are susceptible to hydrolysis under aqueous conditions, causing detachment of the dye from the oxide surface.¹³ The development of dyes for solar cells with a more robust attachment will lead to a more durable and humidity resistant solar cell.

When developing humidity resistant attachments to metal oxides, a potential ligand must bind to metal centers in aqueous conditions. Siderophores, for example, are naturally occurring ligands that are known to bind high oxidation state metals in aqueous conditions.^{14,15} These interactions can even solubilize iron metal from its oxide.¹⁴ These ligands utilize chelating groups including catecholates, α -hydroxycarboxylic acids, and hydroxamic acids to chelate to the metal center.¹⁶ Catecholates have been used to sensitize TiO₂ but are found to be sensitive to oxidation in the presence of oxidants, limiting the overall usefulness of this linkage.¹³ Hydroxycarboxylic acid binding to metal oxides has also been studied but are found to photo-decarboxylate under visible light irradiation.¹⁷ Hydroxamic acids

Department of Chemistry, Yale University, New Haven, Connecticut, 06520-8107. E-mail: victor.batista@yale.edu; charles.schmuttenmaer@yale.edu; gary.brudvig@yale.edu; robert.crabtree@yale.edu

Broader context

The important goal of solar water splitting for fuel production requires linkers and anchors that attach the required photosensitizers and catalysts to a TiO₂ photoanode yet remain stable in an aqueous medium while permitting injection of electrons into the anode. We now report the hydroxamate group as a versatile and effective anchor with these desirable properties.

have only recently been examined for their binding to metal oxide surfaces.^{18,19}

In recent work, we synthesized a ligand with both a terpyridine metal-binding motif and a hydroxamic acid anchoring group to bind to a metal oxide surface (Scheme 1). We demonstrated visible light sensitization of TiO₂ nanoparticles by surface modification with Mn(II)-terpyridine complexes using a hydroxamic acid linker in aqueous environments. By using EPR experiments and THz spectroscopy, we demonstrated that these Mn complexes can be photooxidized with visible light using the TiO₂ nanoparticles as electron acceptors.¹⁹ Additionally, it was shown that the binding of a terpyridine-based molecule with one hydroxamic acid to TiO₂ NPs was more stable under aqueous conditions than the N719 Ru(II) Grätzel dye which presumably binds to TiO₂ through multiple carboxylic acid groups. Furthermore, THz spectroscopy (or pulsed far-infrared spectroscopy) indicated an increased electron injection efficiency when exciting at 400 nm for the hydroxamic acid system compared to N719.¹⁹ Materials with high electrical conductivity absorb far-infrared photons more strongly than materials with low conductivity, and this renders THz spectroscopy a non-contact electrical probe with sub-picosecond time resolution.^{21,22} Because these comparisons were made between two very different systems (a ruthenium dye compared to an organic ligand), a more direct comparison between similar molecules was needed to test these initial results. The synthesis of an analogous Grätzel-type Ru(II) dye bearing a hydroxamic acid anchoring group is also desired to compare solar cell efficiencies.

In this article, we further explore the stability of hydroxamic acid functional groups in their covalent interaction with metal oxide surfaces. The hydroxamic acid group is particularly attractive due to its facile two step synthesis, its known binding to Ti(IV) in aqueous conditions,¹⁶ and its stability when bound to metal oxides over various pH ranges.¹⁸ To draw a direct comparison between a carboxylic acid anchor and a hydroxamic acid, we have synthesized two organic molecules that differ only in their anchoring group. We chose to synthesize azo dyes due to synthetic feasibility and their strong visible absorption. Azo dyes were also chosen to circumvent the problem of hydroxamate reduction that was observed during the synthesis of ruthenium solar dyes. Due to their intense color, we were able to use diffuse reflectance UV-vis spectroscopy to probe the stability in acidic, basic, and neutral aqueous conditions after prolonged exposure. THz spectroscopy was also employed to probe the electron injection dynamics of both azo dyes. We show that the organic dye bearing a hydroxamic acid group was significantly more stable than the corresponding carboxylate in acidic, basic, and neutral aqueous conditions. Furthermore, THz spectra indicated

that the dye with a hydroxamic acid anchor gave comparable injection *versus* the dye bearing a carboxylic acid. These results demonstrate that a hydroxamic acid anchoring group provides more stability when bound to a TiO₂ surface than the conventional carboxylic acid anchor while maintaining efficient IET.

2. Experimental procedures

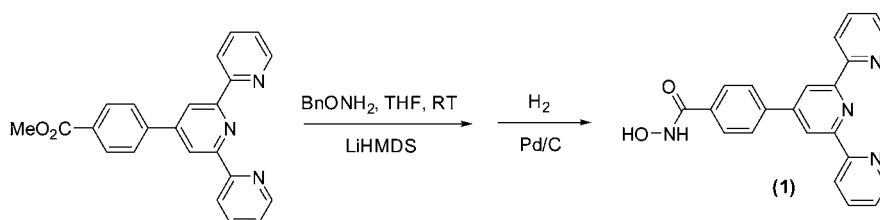
Sample preparation and experimental procedures are described below. All reagents not specifically mentioned were purchased from Aldrich and used without further purification. Ligand synthesis was performed using standard Schlenk techniques under N₂ atmosphere. The ¹H and ¹³C NMR spectra were obtained using Bruker spectrometers operating at 400 and 500 MHz, respectively. Chemical shifts are reported in ppm with the residual solvent as an internal reference. The molecule, **1**, was synthesized by modifying a literature procedure.¹⁹ The Degussa P25 TiO₂ nanoparticles are 25 nm in diameter and are 70% anatase and 30% rutile.

2.1 Synthesis of 4-((4-(dimethylamino)phenyl)diazenyl)benzoic acid (**2**) (Scheme 2).

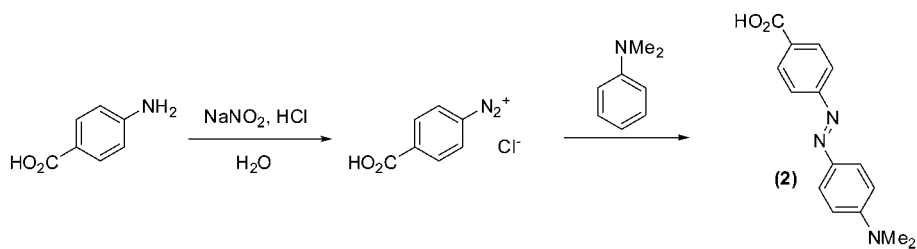
A mixture of 4-aminobenzoic acid (1.51 g, 11.0 mmol) in water was stirred at 0 °C as 12 ml of concentrated HCl was added dropwise. To the previous solution, NaNO₂ (aq) (700 mg, 0.010 mmole in 5 ml H₂O) was added dropwise and stirred for 5 min. During this time an intense red color formed. In a separate flask, a 10% aqueous solution of NaOH (3 g NaOH in 27 mL H₂O) was used to dissolve N,N'-dimethylaniline (1.27 ml, 10.0 mmole) and was cooled to 0 °C. The dissolved N,N'-dimethylaniline was then added slowly to the cooled solution from the reaction of protonated 4-aminobenzoic acid. The resulting solution was allowed to stir at 0 °C for 1 h and was then allowed to reach room temperature while stirring for 12 h. The resulting brick red precipitate was collected by vacuum filtration and recrystallized in methanol to give 1.82 g of product (68% yield). ¹H NMR (DMSO-*d*₆, 400MHz): 8.10–8.06 (d, 2H), 7.86–7.82(m, 4H), 6.84–6.90(d, 2H), 3.09 (s, 6H). ¹³C NMR (DMSO-*d*₆, 500MHz): 166.8, 154.8, 153.0, 142.5, 130.5, 125.3, 121.6, 115.0, 111.7, 39.8. ESI for C₁₅H₁₅N₃O₂⁺: predicted *m/z* = 270.31, observed = 270.30.

2.2 Synthesis of methyl 4-((4-(dimethylamino)phenyl)diazenyl)benzoate (**3**) (Scheme 3).

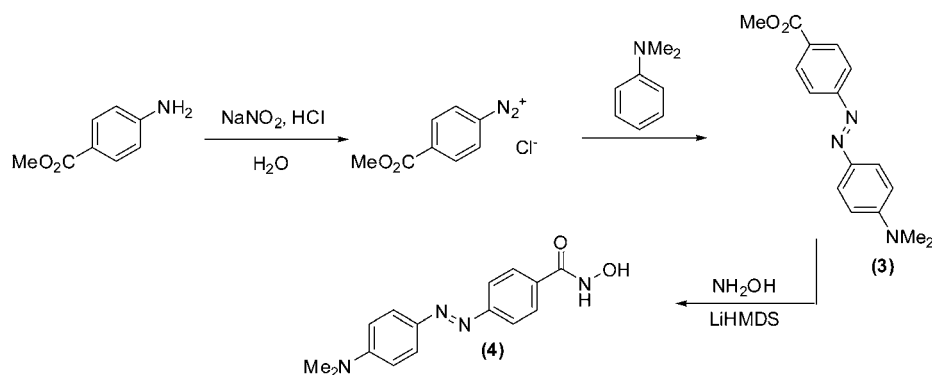
A solution of methyl 4-aminobenzoate (1.00 g, 6.60 mmol) in water was stirred at 0 °C as 12 ml of concentrated HCl was added dropwise. To the previous solution, NaNO₂ (aq) (457 mg,



Scheme 1



Scheme 2



Scheme 3

6.60 mmol) was added dropwise and stirred for 5 min. During this time, a light red coloration was observed. In a separate flask, a 10% aqueous solution of NaOH (3 g NaOH in 27 ml H_2O) was used to dissolve N,N -dimethylaniline and was cooled to 0°C . The dissolved N,N -dimethylaniline solution was then added slowly to the cooled acidic solution from the reaction of 4-aminobenzoate. The resulting solution was allowed to stir at 0°C for 1 h and was then allowed to reach room temperature while stirring for 12 h. The resulting red precipitate was collected by vacuum filtration and recrystallized in methanol to give 780 mg of product (42% yield). ^1H NMR ($\text{DMSO-}d_6$, 400 MHz): 8.07–8.13 (d, 2H), 7.82–7.89 (m, 4H), 6.85–6.90 (d, 2H), 3.89 (s, 3H), 3.10 (s, 6H). ^{13}C NMR (CDCl_3 , 500MHz): 167.2, 160.9, 147.5, 132.2, 131.0, 130.4, 122.0, 115.5, 112.5, 52.6, 41.0. ESI for $\text{C}_{16}\text{H}_{18}\text{N}_3\text{O}_2^+$: predicted $m/z = 284.14$, observed = 284.30.

2.3 Synthesis of 4-((4-(dimethylamino)phenyl)diazanyl)-*N*-hydroxybenzamide (4) (Scheme 3).

A mixture of **3** (200 mg, 0.706 mmole) and hydroxylamine hydrochloride (49 mg, 0.706 mmole) was stirred in 40 ml of dry THF at 0°C . To this solution, excess LiHMDS (3.53 mL of 1.0 M solution) was added. The reaction was allowed to reach room temperature and then stirred overnight. The resulting dark red solution was extracted with ethyl acetate and excess NH_4Cl (aq). The resulting ethyl acetate solution contained product and was dried with magnesium sulfate before removing the solvent under reduced pressure. This afforded 165 mg of product (yield 82%). ^1H NMR ($\text{DMSO-}d_6$, 400 MHz): 7.87–7.90 (d, 2H), 7.77–7.83 (m, 4H), 6.82–6.86 (d, 2H), 3.06 (s, 6H). ^{13}C NMR ($\text{DMSO-}d_6$, 500 MHz): 162.3, 154.4, 153.3, 143.0, 131.8, 125.5, 122.0,

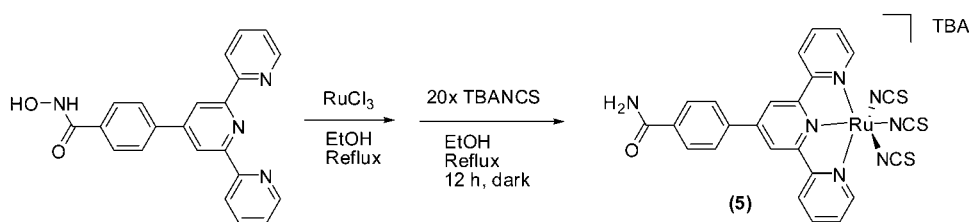
115.7, 111.9, 40.2. ESI for $\text{C}_{15}\text{H}_{17}\text{N}_4\text{O}_2$: calculated $m/z = 285.32$, observed = 285.40.

2.4 Synthesis of (5) (Scheme 4).

The ligand, **1**, was synthesized according to literature procedures.¹⁹ RuCl_3 trihydrate (205 mg, 0.788 mmole) was refluxed in 30 ml ethanol for 30 min. A solution of **1** (290 mg, 0.788 mmole) in 10 ml of degassed ethanol was then transferred into the ruthenium solution and refluxed for 2 h. The resulting solution was then cooled at 0°C for 4 h. The resulting precipitate was then collected and recrystallized in methanol to give 264 mg of the Ru(III) precursor (58% yield). 100 mg (0.174 mmole) of the Ru(III) precursor and excess tertbutylammonium thiocyanate (1.44 g, 3.472 mmole) were refluxed overnight in 20 mL of ethanol in the dark. The resulting purple solution was extracted into dichloromethane and recrystallized in methanol to give 57 mg of **5** (51% yield). ^1H NMR (400 MHz, $\text{DMSO-}d_6$): 9.15 (s, 2H), 8.93–9.05 (m, 4H), 8.45–8.47 (d, 2H), 8.25–8.32 (m, 5H), 7.87–7.95 (t, 2H), 3.25–3.40 (m, 8H), 1.60–1.75 (m, 8H), 1.40–1.50 (m, 8H), 1.09–1.18 (m, 12H). ESI for $\text{C}_{25}\text{H}_{16}\text{N}_7\text{ORuS}_3^-$: calculated $m/z = 627.96$, observed = 627.9638.

2.5 Preparation of mesoporous thin films of sensitized TiO_2

The samples for ultraviolet-visible (UV-vis) and time-resolved Terahertz (THz) spectroscopic measurements consist of mesoporous thin films (~ 5 – $15\ \mu\text{m}$ thick) of Degussa P25 TiO_2 nanoparticles. The nanoparticles were stirred overnight in a ratio of 2 mL H_2O to 1 g nanoparticles. The resulting solution was doctor-bladed onto a glass coverslip and annealed in air at 450°C for 2 h with a ramp rate of 5°C min^{-1} . The resulting slides were sensitized with adsorbate by submerging the sample slide in



Scheme 4

a 20 mM solution of **2** or **4** for 2 h. The sensitized films, denoted as **2**-TiO₂ and **4**-TiO₂, respectively, were rinsed with ethanol then dry dichloromethane and dried under a stream of N₂ gas.

2.6 Water stability studies by UV-vis spectrophotometry

Samples of **2**-TiO₂ and **4**-TiO₂ were submerged in deionized neutral pH water for varying amounts of time. Once removed from the water solution, the slides were rinsed with additional deionized water and dried under a stream of N₂ gas for 5 min before recording the spectra. For acid stability studies, the samples of **2**-TiO₂ and **4**-TiO₂ were submerged in pH 2.0 HCl for varying amounts of time, were rinsed with deionized water, and dried under a stream of N₂ gas for 5 min. For base stability studies, the samples were submerged in a pH 10.25 K₂CO₃ solution for varying amounts of time, rinsed with deionized water, and dried under a stream of N₂ before recording the spectra.

2.7 UV-Vis and FT-IR measurements

Films of TiO₂ nanoparticles are highly scattering, so spectra were obtained with a Varian Cary 3 spectrophotometer in diffuse reflectance geometry using an integrating sphere. Diffuse reflectance Fourier transform infrared (FTIR) spectra were recorded with a deuterated triglycine sulfate (DTGS) detector and a Nexus Smart Collector. Samples were collected as dry materials and measured in a KBr pellet. Typically, 128 scans were performed for each spectrum. The resolution was 2 cm⁻¹. Analogous FTIR methods were previously applied to characterize the binding of carboxylate linkers on Degussa P25 TiO₂ NPs.²⁰

2.8 Time-resolved terahertz spectroscopy measurements

An amplified Ti:sapphire laser (Tsunami/Spitfire from Spectra Physics) generated 800 mW of pulsed near-IR light at a 1 kHz repetition rate. The pulse width was ~100 fs, and the center wavelength was 800 nm. Roughly two-thirds of the power was frequency doubled and then filtered to produce 50 mW of 400 nm (3.10 eV) light for the pump beam. The remainder of the near-IR light was used to generate and detect THz radiation using a 4-paraboloid arrangement that focused the THz beam to a spot size of ~3 mm at the sample. Terahertz radiation was generated using optical rectification in a ZnTe(110) crystal and detected using free space electrooptic sampling in a second ZnTe(110) crystal. Terahertz data were taken at room temperature. The sample position was varied during scanning to prevent bleaching of the dye and to minimize inconsistencies due to sample

thickness. Further information on the spectrometer and techniques has been reported in the literature.^{21,22}

Terahertz radiation is absorbed by mobile electrons in the TiO₂ conduction band and is insensitive to electrons within the absorbed sensitizer. A decrease in broadband THz (0.2 to 2.5 THz, or equivalently, 6.7 to 83 cm⁻¹) transmission in photoexcited samples compared to nonphotoexcited samples indicates a higher electron density in the TiO₂. Injection time was measured by monitoring the change in THz transmission as the delay time between the 400 nm pump and the THz probe was varied.

2.9 Computational methods

The simulated UV-vis spectrum of **4** was computed using the time dependent-density functional theory (TD-DFT) computational method.^{23,24} The TD-DFT calculations were performed using Gaussian 03 with the B3LYP density functional and 6-31G(d) basis set.^{25–28} The geometry of **4** was relaxed to the optimum structure in vacuum at the B3LYP/6-31G(d) level of theory. The resulting spectra were obtained by convolution of each set of discrete transitions with a Gaussian function (FWHM = 70 nm) to mimic inhomogeneous broadening induced by thermal nuclear fluctuations. The oscillator strengths were used to assign relative weights to the transitions and the total absorbance was globally scaled to facilitate comparison with the experimental UV-vis spectra.

3. Results

The results are presented in three subsections. First we have analyzed the water, base, and acid stability of our organic sensitizers on TiO₂ which differ in only the anchoring functional group. We then compared the electron injection capabilities of both molecules using THz spectroscopy. Finally, we discuss attempts to synthesize a ruthenium dye with a hydroxamic acid linkage to develop a more humidity resistant solar cell.

3.1 Stability studies of the organic dyes under various aqueous conditions

Previously, we have reported the water stability of a terpyridine ligand (**1**) on TiO₂ compared to the stability of Grätzel's red dye (N719) bound to TiO₂.¹⁹ Due to the higher solubility of N719 in water than our hydrophobic terpyridine ligand, it is possible that solvation played a role in the detachment of N719 from TiO₂. To avoid this problem, we have now synthesized two organic molecules which differ only in the anchoring functional group (Schemes 2 and 3). We then sensitized TiO₂ with these molecules

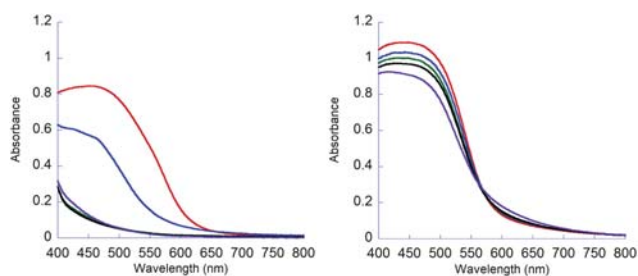


Fig. 1 *Left:* UV-visible spectra of **2**-TiO₂ after exposure to pH 6.5 deionized water for 0 h (red), 1 h (blue), 2 h (green), 6 h (black), and 24 h (purple). *Right:* UV-visible spectra of **4**-TiO₂ after exposure to water for 0 h (red), 1 h (blue), 2 h (green), 6 h (black), and 24 h (purple).

and exposed the sensitized nanoparticles to water for varying amounts of time. Fig. 1 shows the UV-vis spectra of both the carboxylic acid bound to TiO₂ (**2**-TiO₂) and the hydroxamic acid bound to TiO₂ (**4**-TiO₂) after exposure to deionized water over varying amounts of time. After incubation in water, a large decrease in absorbance is observed for **2**-TiO₂ attached through the carboxylic acid. This decrease in absorbance suggests a substantial leaching of dye from the TiO₂ surface after only 2 h of water exposure. In contrast, after 24 h of incubation in water, there seems to be an insignificant change in the amount of **4** bound to the surface of TiO₂, as reflected by the isosbestic point at 580 nm, but there does appear to be a slight spectral change.

For the purpose of using homogeneous catalysts that can be immobilized on metal oxides for enhanced reactivity and recyclability, stability of linkages under basic conditions becomes important. Specifically, many processes related to hydrogen transfer reactions rely on stoichiometric or catalytic amounts of base, posing a severe challenge for existing linker technology.²⁹ With this in mind we tested the stability of the **4**-TiO₂ and **2**-TiO₂ after incubation in a solution of K₂CO₃ at pH 10.25. Fig. 2 shows the UV-vis spectra of samples of **2**-TiO₂ and **4**-TiO₂ after exposure to this solution over varying amounts of time. Fig. 2 shows the complete detachment of **2**-TiO₂ under basic conditions after 2 h of incubation. In contrast, an insignificant change in the amount of **4**-TiO₂ was seen after 24 h of incubation under basic conditions, again reflected by the isosbestic point at 580 nm.

As noted above, the stability studies display an isosbestic point at 580 nm for **4**-TiO₂ at neutral pH (Fig. 1) and basic pH (Fig. 2).

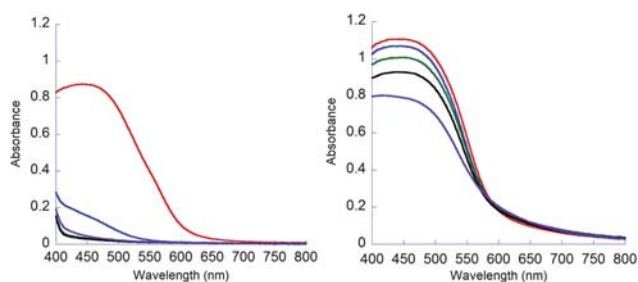


Fig. 2 *Left:* UV-visible spectra of **2**-TiO₂ after exposure to water for 0 h (red), 1 h (blue), 2 h (green), 6 h (black), and 24 h (purple). *Right:* UV-visible spectra of **4**-TiO₂ after exposure to pH 10.25 K₂CO₃ for 0 h (red), 1 h (blue), 2 h (green), 6 h (black), and 24 h (purple).

This suggests that the protonation state is changing after varying amounts of time under these conditions.

Many current homogenous water oxidation systems utilize primary oxidants such as ceric ammonium nitrate which are only stable under highly acidic conditions.³⁰ Due to the pH dependence of these systems, it is crucial that a linkage be stable under acidic conditions if a metal catalyst is to be immobilized on TiO₂ for the purposes of developing a photocatalytic water splitting cell. The stability of **2**-TiO₂ and **4**-TiO₂ were therefore compared after incubation in acidic conditions (pH 2.0 HCl) for varying amounts of time. Fig. 3 shows the UV-vis spectra of the sensitized nanoparticles after exposure to these conditions. In comparison to neutral (Fig. 1) or basic (Fig. 2) conditions, it is apparent that **2**-TiO₂ is more stable under acidic conditions. Nonetheless, after 24 h of incubation in acidic solution, **4**-TiO₂ is more robust.

Fig. 4 shows a plot of the relative absorbances at 580 nm of these samples after various incubation times under basic and neutral pH. The results show a dramatic decrease in absorbance for the dye anchored with carboxylic acid (blue) compared to the dye anchored with the hydroxamic acid (red). This suggests that very little of **4** is detaching from TiO₂ under the experimental conditions, whereas **2** dissociates rapidly.

3.2 Ultrafast interfacial electron transfer

Because radiation at terahertz frequencies is absorbed by mobile electrons but not localized electrons, Time-resolved terahertz spectroscopy (TRTS), an optical pump/THz probe technique, is useful for determining the speed and relative efficiency of

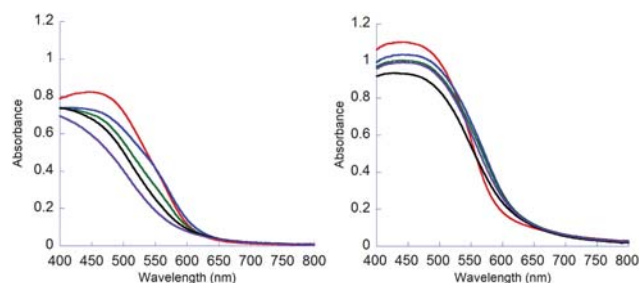


Fig. 3 *Left:* UV-visible spectra of **2**-TiO₂ after exposure to water for 0 h (red), 1 h (blue), 2 h (green), 6 h (black), and 24 h (purple). *Right:* UV-visible spectra of **4**-TiO₂ after exposure to pH 2.0 HCl for 0 h (red), 1 h (blue), 2 h (green), 6 h (black), and 24 h (purple).

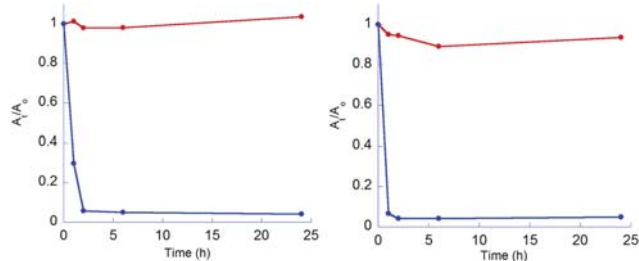


Fig. 4 Relative A_t/A_0 absorbance ratio of **2**-TiO₂ (blue) and **4**-TiO₂ (red) at 580 nm after incubation in water (left) and K₂CO₃ solution (right) for varying amounts of time.

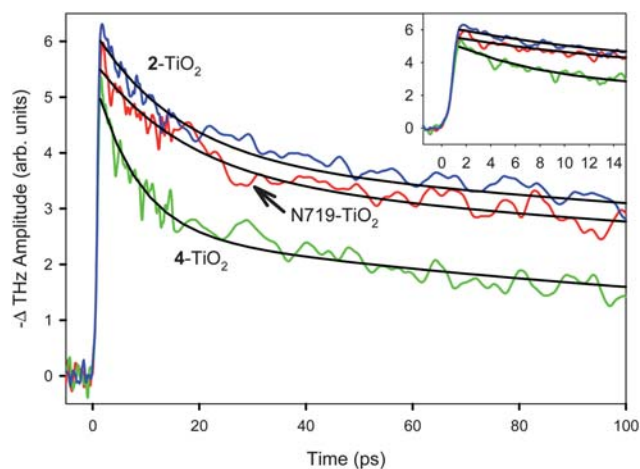


Fig. 5 400 nm pump/THz probe of electron injection in functionalized TiO₂ NP films of the following: **2** (blue), **4** (green), and N719 (red).

electron injection into nanoparticulate semiconductors.^{21,22} Fig. 5 shows ultrafast interfacial electron injection induced by 400 nm photoexcitation of TiO₂ NP colloidal thin films made of **2**-TiO₂, **4**-TiO₂, and N719-TiO₂. The ultrafast spectroscopic data indicate that IET from the adsorbate to the NP after photoexcitation of the system is completed within the ~500 fs time resolution for the spectrometer (inset of Fig. 5). THz measurements taken over hundreds of picoseconds do not show any slower injection components for any of the sensitizers.

The initial magnitude of the changes in THz transmission through all three samples is essentially the same (see inset of Fig. 5). Although the transmission unit in Fig. 5 is arbitrary, the same scaling factor is used for all spectra, so amplitude comparisons are meaningful. However, on longer time scales it is seen that the change in THz transmission signal is a double exponential decay, and was fitted with the following functional form:

$$-\Delta THz = Offset + A_1 e^{-t/\tau_1} + A_2 e^{-t/\tau_2} \quad (1)$$

where ΔTHz is the change in THz transmission amplitude, *Offset* is the change in THz amplitude at long times (greater than 1 ns), A_1 and A_2 are the amplitudes of the components of the double exponential, and τ_1 and τ_2 are their time constants. The fitted parameters are given in Table 1.

The behavior of **2**-TiO₂ is almost identical to N719-TiO₂. They each have a fast time constant of roughly 17 ps and a slow one of 300 ps, and their relative amplitudes are about the same wherein the amplitude of the slower time constant is slightly larger than that of the fast one. On the other hand, **4**-TiO₂ behaves differently. The fast time constant is 8.0 ps, and the slow one is 160 ps, each of which are about a factor of two faster than the other two samples, and amplitude of the faster time constant is larger than

Table 1 Results of fitting eqn (1) to the experimental data

Sample	<i>Offset</i>	A_1	τ_1 /ps	A_2	τ_2 /ps
N719-TiO ₂	0.97	2.2	17.4	2.5	285
2 -TiO ₂	0.93	2.4	16.0	2.9	328
4 -TiO ₂	0.44	2.9	8.0	2.2	160

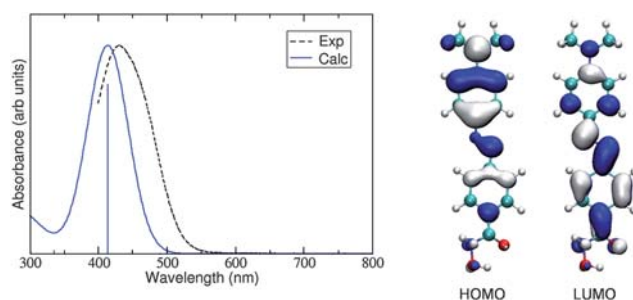


Fig. 6 Comparison of the simulated UV-vis spectrum of **4** in vacuum with the experimental spectrum obtained in ethanol at neutral pH (left) and isosurfaces of the HOMO and LUMO frontier orbitals of **4** computed at the B3LYP/6-31G(d) level of theory (right).

that of the slower one. Also, the electron density in the TiO₂ decays to a lower level in **4**-TiO₂ relative to the other two samples.

3.3 Computational results

Fig. 6 shows the TD-DFT spectrum for **4** in vacuum. A visible light absorption band is found at ~414 nm corresponding to a single HOMO–LUMO transition. Other transitions are observed but they occur below 400 nm in the UV region. The simulated UV-vis spectrum is in good agreement with the experimental spectrum of **4**, measured in ethanol at neutral pH (see Fig. 6), showing a transition centered at ~430 nm. From the DFT results, we can assign the visible absorption band as a π – π^* transition from the HOMO to LUMO. The DFT HOMO and LUMO frontier orbitals are displayed in Fig. 6.

3.4 Attempted synthesis of ruthenium dyes for DSSCs

In an effort to utilize the hydroxamic acid linkage in DSSCs, a ruthenium dye bearing this linkage, [nBu₄][Ru(NCS)₃(**1**)], was desired to compare the efficiency and stability of such a system to established systems containing carboxylic acid anchoring groups.² The first synthetic procedure we employed proceeds through a protected hydroxamic acid intermediate bearing a benzyl protection group. However, the subsequent deprotection of the hydroxamic acid resulted in decomposition of the ruthenium complex. A more straightforward synthesis was employed using the unprotected hydroxamic acid (Scheme 4) and proceeded with good yield. However, a reduction occurred during the synthesis resulting in the reduction of the hydroxamic acid to an amide. Other synthetic methodologies were employed including a more mild chloride abstraction with AgNCS. Other synthetic procedures also resulted in the amide product (**5**). Although **5** sensitized TiO₂, solar cells of the complex suffered from poor efficiency due to poor surface coverage resulting from weak anchoring of **5** to TiO₂.

4. Conclusions

The design and synthesis of two dye molecules differing only in anchoring motif has allowed us to draw a direct comparison between hydroxamate and carboxylate anchoring groups for sensitizing TiO₂. We show that derivatized hydroxamic acid

groups function as more robust linkages for TiO₂ than carboxylates over a broad pH range. These results suggest that hydroxamic acid anchors will provide a versatile covalent attachment to TiO₂ surfaces. The experimental results are consistent with our prior computational data suggesting that hydroxamate anchors are 20% more stable (~6 kcal mol⁻¹) than carboxylate when attached to TiO₂ surfaces.¹⁹ Hydroxamate groups could be particularly useful in attaching transition metal complexes to metal oxide semiconductors. Their stability in acidic conditions when bound to TiO₂ also makes them an attractive choice for an anchoring motif when designing cells for photocatalytic water splitting applications. The stability of these attachments under basic conditions highlights their applicability in designing recyclable catalysts bound to metal oxides for hydrogen transfer or other catalytic reactions. Similarly, dyes synthesized with hydroxamate functionalities replacing less robust carboxylate groups could aid in the development of humidity resistant solar cells.

The numerous synthetic methodologies available for assembling hydroxamic acid groups may allow these systems to be implemented for numerous applications. As shown in our attempts to synthesize Ru(II) dyes for solar cell applications, it is important to note the possibility of reduction to give an undesired amide product. Numerous synthetic methodologies were employed to obtain a ruthenium dye with a hydroxamic acid group, but all converged on the final amide product. However, it may be possible to circumvent this complication by proceeding through a protected hydroxamate intermediate, or through introduction of the hydroxamate functionality at the final step. The observation of ultrafast IET through this linkage reinforces its usefulness in anchoring molecules to metal oxide surfaces. Considering stability, ease of synthesis, and electron injection characteristics, hydroxamic acids improve upon conventional carboxylic acid linkages for providing robust sensitization of TiO₂.

Acknowledgements

The authors acknowledge support from the Chemical Sciences, Geosciences, and Biosciences Division, Office of Basic Energy Sciences, Office of Science, U.S. Department of Energy (DE-FG02-07ER15909) and DOE supercomputer time from NERSC. Also, NSF ECCS-0404191 grant supported preliminary work. This research was in part supported by the US Department of Energy, Office of Basic Energy Sciences as part of the ANSER Energy Frontier Research Center. W.M. thanks Kathleen L. Batchler and Prof. Ann M. Valentine for helpful discussion.

References

- 1 B. O'Regan and M. Grätzel, *Nature*, 1991, **353**, 737–740.
- 2 M. K. Nazeeruddin, A. Kay, I. Rodicio, R. Humphrybaker, E. Muller, P. Liska, N. Vlachopoulos and M. Grätzel, *J. Am. Chem. Soc.*, 1993, **115**, 6382–6390.
- 3 N. Serpone, *Res. Chem. Intermed.*, 1994, **20**, 953–992.
- 4 S. G. Abuabara, C. W. Cady, J. B. Baxter, C. A. Schmuttenmaer, R. H. Crabtree, G. W. Brudvig and V. S. Batista, *J. Phys. Chem. C*, 2007, **111**, 11982–11990.
- 5 I. Martini, J. H. Hodak and G. V. Hartland, *J. Phys. Chem. B*, 1999, **103**, 9104–9111.
- 6 Y. X. Weng, Y. Q. Wang, J. B. Asbury, H. N. Ghosh and T. Q. Lian, *J. Phys. Chem. B*, 2000, **104**, 93–104.
- 7 Z. F. Chen, J. J. Concepcion, J. W. Jurss and T. J. Meyer, *J. Am. Chem. Soc.*, 2009, **131**, 15580–15581.
- 8 P. W. Du, J. Schneider, G. G. Luo, W. W. Brennessel and R. Eisenberg, *Inorg. Chem.*, 2009, **48**, 8646–8646.
- 9 W. J. Youngblood, S. H. A. Lee, Y. Kobayashi, E. A. Hernandez-Pagan, P. G. Hoertz, T. A. Moore, A. L. Moore, D. Gust and T. E. Mallouk, *J. Am. Chem. Soc.*, 2009, **131**, 926–927.
- 10 Photochemical conversion and storage of solar energy, J. S. Connolly (ed.), Academic Press, New York, 1981.
- 11 C. F. Zou and M. S. Wrighton, *J. Am. Chem. Soc.*, 1990, **112**, 7578–7584.
- 12 I. Haller, *J. Am. Chem. Soc.*, 1978, **100**, 8050–8055.
- 13 W. R. McNamara, R. C. Snoberger, G. Li, J. M. Schleicher, C. W. Cady, M. Poyatos, C. A. Schmuttenmaer, R. H. Crabtree, G. W. Brudvig and V. S. Batista, *J. Am. Chem. Soc.*, 2008, **130**, 14329–14338.
- 14 C. Cocozza, C. C. G. Tsao, S. F. Cheah, S. M. Kraemer, K. N. Raymond, T. M. Miano and G. Sposito, *Geochim. Cosmochim. Acta*, 2002, **66**, 431–438.
- 15 R. T. Reid, D. H. Live, D. J. Faulkner and A. Butler, *Nature*, 1993, **366**, 455–458.
- 16 R. Uppal, H. P. Israel, C. D. Incarvito and A. M. Valentine, *Inorg. Chem.*, 2009, **48**, 10769–10779.
- 17 I. A. Shkrob and S. D. Chemerisov, *J. Phys. Chem. C*, 2009, **113**, 17138–17150.
- 18 J. Yang, P. J. Bremer, I. L. Lamont and A. J. McQuillan, *Langmuir*, 2006, **22**, 10109–10117.
- 19 W. R. McNamara, R. C. Snoberger, G. H. Li, C. Richter, L. J. Allen, R. L. Milot, C. A. Schmuttenmaer, R. H. Crabtree, G. W. Brudvig and V. S. Batista, *Energy Environ. Sci.*, 2009, **2**, 1173–1175.
- 20 C. B. Mendive, D. W. Bahnemann and M. A. Blesa, *Catal. Today*, 2005, **101**, 237–244.
- 21 J. B. Baxter and C. A. Schmuttenmaer, *J. Phys. Chem. B*, 2006, **110**, 25229–25239.
- 22 (a) M. C. Beard, G. M. Turner and C. A. Schmuttenmaer, *Phys. Rev. B: Condens. Matter Mater. Phys.*, 2000, **62**, 15764–15777; (b) G. M. Turner, M. C. Beard and C. A. Schmuttenmaer, *J. Phys. Chem. B*, 2002, **106**, 11716–11719.
- 23 R. E. Stratmann and G. E. Scuseria, *Abstracts of Papers of the American Chemical Society*, 1998, **215**, U259–U259.
- 24 M. E. Casida, C. Jamorski, K. C. Casida and D. R. Salahub, *J. Chem. Phys.*, 1998, **108**, 4439–4449.
- 25 M. J. Frisch, G. W. Trucks, H. B. Schlegel, G. E. Scuseria, M. A. Robb, J. R. Cheeseman, J. A. Montgomery, Jr., T. Vreven, K. N. Kudin, J. C. Burant, J. M. Millam, S. S. Iyengar, J. Tomasi, V. Barone, B. Mennucci, M. Cossi, G. Scalmani, N. Rega, G. A. Petersson, H. Nakatsuji, M. Hada, M. Ehara, K. Toyota, R. Fukuda, J. Hasegawa, M. Ishida, T. Nakajima, Y. Honda, O. Kitao, H. Nakai, M. Klene, X. Li, J. E. Knox, H. P. Hratchian, J. B. Cross, V. Bakken, C. Adamo, J. Jaramillo, R. Gomperts, R. E. Stratmann, O. Yazyev, A. J. Austin, R. Cammi, C. Pomelli, J. Ochterski, P. Y. Ayala, K. Morokuma, G. A. Voth, P. Salvador, J. J. Dannenberg, V. G. Zakrzewski, S. Dapprich, A. D. Daniels, M. C. Strain, O. Farkas, D. K. Malick, A. D. Rabuck, K. Raghavachari, J. B. Foresman, J. V. Ortiz, Q. Cui, A. G. Baboul, S. Clifford, J. Cioslowski, B. B. Stefanov, G. Liu, A. Liashenko, P. Piskorz, I. Komaromi, R. L. Martin, D. J. Fox, T. Keith, M. A. Al-Laham, C. Y. Peng, A. Nanayakkara, M. Challacombe, P. M. W. Gill, B. G. Johnson, W. Chen, M. W. Wong, C. Gonzalez and J. A. Pople, *GAUSSIAN 03 (Revision B.04)*, Gaussian, Inc., Wallingford, CT, 2004.
- 26 A. D. Becke, *J. Chem. Phys.*, 1993, **98**, 5648–5652.
- 27 W. J. Hehre, R. Ditchfie and J. A. Pople, *J. Chem. Phys.*, 1972, **56**, 2257–2261.
- 28 P. C. Hariharan and J. A. Pople, *Theor. Chim. Acta*, 1973, **28**, 213–222.
- 29 G. E. C. Dobreiner and R. H. Crabtree, *Chem. Rev.*, 2010, **110**, 681–703.
- 30 J. F. Hull, D. Balcells, J. D. Blakemore, C. D. Incarvito, O. Eisenstein, G. W. Brudvig and R. H. Crabtree, *J. Am. Chem. Soc.*, 2009, **131**, 8730–8731.